electronics

MDPI

Article

Mathematical Model of a Semiconductor Structure Based on Vanadium Dioxide for the Mode of a Conductive Phase

Oleksii Kachura [1], Valeriy Kuznetsov [2,*], Mykola Tryputen [3], Vitalii Kuznetsov [4,*], Sergei Kolychev [1], Artur Rojek [2] and Petro Hubskyi [2]

[1] Faculty of Computer Technology and Energy, Dniprovsky State Technical University, Dniprobudivska Street 2, 51900 Kamianske, DR, Ukraine; fem@ukr.net (O.K.); kolychev.sergey58@gmail.com (S.K.)
[2] Railway Research Institute, 50 Józefa Chłopickiego Street, 04-275 Warsaw, Poland; arojek@ikolej.pl (A.R.); phubskyi@ikolej.pl (P.H.)
[3] Department of Cyberphysical and Information-Measuring Systems, Faculty of Electrical Engineering, Institute of Power Engineering, Dnipro University of Technology, 19 Dmytro Yavornytskyi Avenue, 49005 Dnipro, DR, Ukraine; nikolay.triputen@gmail.com
[4] Department of Electrical Engineering, Faculty of Electomechanic and Electrometallurgy, Dnipro Metallurgical Institute, Ukrainian State University of Science and Technologies, 2 Lazaryana Street, 49000 Dnipro, DR, Ukraine
* Correspondence: vkuznetsov@ikolej.pl (V.K.); witjane20002014@gmail.com (V.K.)

Abstract

This study presents a comprehensive mathematical model of a semiconductor structure based on vanadium dioxide (VO_2), specifically in its conductive phase. The model was developed using the finite element method (FEM), enabling detailed simulation of the formation of a conductive channel under the influence of low-frequency alternating voltage (50 Hz). The VO_2 structure under investigation exhibits pronounced electric field concentration at the surface, where the field strength reaches approximately 5×10^4 V/m, while maintaining a more uniform distribution of around 2×10^4 V/m within the bulk of the material. The simulation results were validated experimentally using a test circuit. Minor deviations—no greater than 8%—were observed between the simulated and measured current values, attributed to magnetic core saturation and modeling assumptions. A distinctive feature of the model is its ability to incorporate the nonlinear dependencies of VO_2's electrical properties on frequency. Analytical expressions were derived for the magnetic permeability and resistivity of VO_2, demonstrating excellent agreement with experimental data. The coefficients of determination (R^2) for the frequency dependence of magnetic permeability and resistance were found to be 0.9976 and 0.9999, respectively. The current version of the model focuses exclusively on the conductive phase and does not include the thermally induced metal–insulator phase transition characteristic of VO_2. The study confirms that VO_2-based structures exhibit high responsiveness and nonlinear switching behavior, making them suitable for applications in electronic surge protection, current limiting, and switching elements. The developed model provides a reliable and physically grounded tool for the design and optimization components based on VO_2 in power electronics and protective circuitry.

Keywords: vanadium dioxide; finite element method; electric field strength; semiconductor modeling; nonlinear conductivity; magnetic permeability; phase transition; current surge protection; experimental validation

Academic Editor: Nakkeeran Kaliyaperumal

Received: 21 May 2025
Revised: 5 July 2025
Accepted: 7 July 2025
Published: 18 July 2025

Citation: Kachura, O.; Kuznetsov, V.; Tryputen, M.; Kuznetsov, V.; Kolychev, S.; Rojek, A.; Hubskyi, P. Mathematical Model of a Semiconductor Structure Based on Vanadium Dioxide for the Mode of a Conductive Phase. *Electronics* **2025**, *14*, 2884. https://doi.org/10.3390/electronics14142884

1. Introduction

Starting currents in electronic devices connected to power supplies can trigger critical mode transitions, leading to failure. To mitigate this, protective measures are essential to lessen peak current values and prolong equipment lifespan. Contemporary protection devices must be uncomplicated, dependable, and cost-effective. One such solution employs vanadium dioxide (VO_2)-based structures, which are integrated in series with the load. Thermistors, in particular, have emerged as highly efficient components for this purpose [1–5].

Vanadium dioxide structures offer a robust defense against excessive current surges. These devices swiftly respond to abrupt changes in current, effectively limiting the impact on the connected electronic equipment. By strategically incorporating VO_2-based components, systems gain enhanced resilience without compromising simplicity or cost-effectiveness. Critical thermistors, owing to their unique thermal properties, stand out as the optimal choice, providing reliable protection against adverse current fluctuations. In essence, the utilization of VO_2-based structures and critical thermistors exemplifies a sophisticated yet practical approach to safeguarding electronic devices from potential damage caused by starting currents and critical mode transitions [6–12]. For example, a recent study [13] supports this idea by highlighting the ultrafast phase transition properties of VO_2, which enable its application as an effective current surge limiter. The article by [13] notes that VO_2 can switch states within nanoseconds under current stress, effectively mimicking the behavior of thermistors. VO_2-based devices also demonstrate high endurance (over 260 million cycles) and can be manufactured using low-cost methods like inkjet printing. Their sharp thermal response and electrical nonlinearity make them highly effective for protecting electronics from surge currents without complicating system design [13].

Building on this, the study [14] demonstrates the strong potential of VO_2-based devices for effective surge protection. The authors introduce a two-terminal configuration using multiple VO_2 microbridges, which enables fast and reversible switching triggered by current or voltage. This multibridge design enhances switching stability and maintains reliable performance over numerous cycles. Thanks to localized Joule heating, the device limits current efficiently, functioning similarly to thermistors. Its simple structure and compatibility with low-cost fabrication methods make it a promising solution for compact and scalable electronic protection systems [14].

Further supporting this concept, the study [15] demonstrates that VO_2-based metal–oxide–metal devices exhibit fast, reversible switching on nanosecond timescales, making them suitable for surge protection. Devices with nanoscale channels show stable switching at threshold voltages and support oscillation frequencies up to 300 MHz. The authors highlight that VO_2 transitions are driven by localized Joule heating and act as self-resetting fuses, with lower power requirements at smaller scales. These findings confirm VO_2's effectiveness as a compact, cost-efficient, and reliable current-limiting solution [15].

These studies consistently demonstrate that VO_2 combines speed, sensitivity, and stability, making it highly effective for protecting electronic circuits from electrical stress. Such findings not only validate its practical use in surge protection but also highlight its broader potential in advanced functional materials.

Vanadium dioxide, classified among transition metal oxides, holds immense promise as a material for electronic functional elements. Its unique properties, including a metal–insulator transition near room temperature, make it highly adaptable for various applications in electronics. VO_2 exhibits remarkable conductivity changes in response to external stimuli like temperature, electric fields, and light, rendering it suitable for innovative electronic devices. Researchers are exploring its potential in fields such as memory devices, sensors, and smart windows. The versatility and tunability of vanadium dioxide position

it as a frontrunner in the development of next-generation electronic components, paving the way for more efficient, responsive, and versatile technologies [8,16–19]. Its unusual properties arise from strong correlations of electrons, which lead to the formation of a metal–semiconductor phase transition (MSPT) under certain conditions [12,20–22]. This process occurs at a temperature of T = 340 K and is accompanied by a change in the electrical conductivity of the structure by up to five orders of magnitude [13,23,24]. At the same time, the parameters of the transition depend on various factors, in particular, the presence of impurities and defects [25–27]. Additionally, vanadium dioxide, like some other transition metal oxides, exhibits the phenomenon of electrical switching associated with MSPT—a rapid change in the system's conductivity under the action of an electric field [8–10,28–32]. This makes it possible to synthesize fast-acting innovative materials of modern electronics [6,7,16,17,33] (temperature sensors, optical switches, memory elements, energy-saving coating, optical information carriers, thermochromic indicators) and manufacture various protective devices, such as switching elements and critical thermistors [8,34,35] (thermistors operating at the phase transition temperature). The latter are used in temperature stabilization and regulation circuits, as well as for protecting electronic devices from inrush currents and pulse signals.

These physical effects form the basis for a wide range of innovative applications. To better understand and optimize VO_2-based devices, recent research has focused on the interplay between thermal and electrical mechanisms driving the phase transition.

Recent research provides a deeper understanding of the dual nature—thermal and electrical—of the metal–insulator phase transition (MIT) in VO_2. The authors of [36] demonstrated that tungsten doping and oxygen vacancy engineering significantly affect the transition temperature and hysteresis width, confirming the key role of structural imperfections in determining phase behavior. Moreover, the authors of [14] studied VO_2-based multibridge switching devices and showed that current-induced transitions closely replicate thermal transitions, but occur via localized Joule heating—emphasizing the electrical control aspect of MIT.

Importantly, the authors of [13] highlighted that the transition in VO_2 can occur on nanosecond or even sub-nanosecond timescales, with initial electronic changes preceding the structural transformation. This supports the widely accepted Mott–Peierls cooperative model of the transition, where electron correlations and lattice distortions act together. These findings not only explain the mechanism of electrical switching in VO_2 but also justify its use in critical thermistors, self-resetting surge protectors, and other fast-response electronic components.

The sensitivity of the MIT in VO_2 to defects, doping, and external excitation makes it a highly tunable material. Its ability to combine sharp conductivity switching with thermal and electrical control mechanisms makes vanadium dioxide a promising candidate for the development of next-generation functional devices.

To fully harness this potential in practical applications, it is essential to not only study VO_2-based elements experimentally but also to develop accurate models that describe their behavior under combined electrical and thermal influence.

Studies [29] have shown that elements based on VO_2 have an S-shaped volt–ampere characteristic and are capable of passing an electric current up to 10 A/cm^2 for a long time after switching to a low-resistance state. This is a significant advantage over conventional semiconductor elements. In [30], the temperature characteristics of elements based on dioxide vanadium were experimentally investigated, and a mathematical model was developed that adequately describes the volt–ampere characteristic of the metal phase channel and the area with negative differential resistance.

A substantial foundation of numerical methods developed for semiconductor device simulation provides a robust methodological basis that can be effectively adapted for modeling VO_2-based structures. Classical finite element and finite volume frameworks pioneered by the authors of [36,37] introduced upwind-stabilized schemes and multigrid Newton solvers that remain the standard strategy for strongly nonlinear drift–diffusion problems. The authors of [38] later extended these ideas with mixed FEM formulations for coupled Poisson and continuity equations, while researchers [39] demonstrated fully three-dimensional FEM solutions that included impact ionization and mesh adaptivity [39]. Although these studies were developed for silicon devices, the mathematical principles—robust stabilization of convection–diffusion terms and self-consistent electro-thermal coupling—are precisely those required to capture the sharp resistive collapse and intense local heating that accompany the VO_2 phase transition. Complementing these numerical advances, the authors of [40] provided benchmark data that distinguish surface from bulk conductivity in VO_2 films, delivering boundary conditions indispensable for quantitative calibration of FEM models.

During the past five years, the classical toolbox has been enriched by a series of VO_2-specific multiphysics studies. The authors of [41] showed, through three-dimensional thermo-elastic FEM, that cyclic switching can concentrate stress at grain boundaries and provoke delamination [41]. On the optical side, the authors of [42] embedded temperature- and field-dependent permittivity into a full-wave FEM of VO_2 metasurfaces, achieving sub-picosecond modulation depths unattainable with simpler, isothermal models [42]. The authors of [43] went further, linking electromagnetic and thermal solvers to design THz absorbers whose resonance shifts exceeded 40% upon modest heating, thereby supplying experimentally validated optical conductivity datasets for model calibration [43]. Collectively, these investigations demonstrate that only a fully coupled description—one that updates conductivity and permittivity with temperature and electric fields—can predict the rich spectrum of VO_2 phenomena, from S-shaped I–V curves to optical modulation and thermo-elastic fatigue.

Taken together, the accumulated experimental evidence and recent progress in numerical modeling highlight not only the remarkable functional potential of VO_2-based devices, but also the persistent absence of a unified quantitative framework capable of fully capturing their complex behavior. While contemporary electro-thermal and opto-thermal simulations can successfully reproduce specific effects—such as nanosecond-scale switching, localized thermo-mechanical stress, and ultrafast optical modulation—these advances remain largely fragmented across separate modeling approaches. This methodological disintegration underscores the pressing need for a comprehensive mathematical model capable of simultaneously resolving the coupled electrical, thermal, and mechanical responses that define VO_2 dynamics.

Building on the body of research on vanadium dioxide semiconductor structures, it is therefore evident that the formulation of such a unified framework remains an open and relevant challenge. The present study aims to address this gap by introducing a finite-element-based model that consistently describes the strongly coupled electro-thermal behavior of VO_2 in dynamic regimes. This approach provides a versatile computational platform for both the performance optimization of functional devices and the development of future multiphysics simulations.

2. Materials and Methods

For a mathematical description of the processes taking place in the VO_2 structure, we used Gauss's theorem, which expresses the relationship between the electric displacement vector and the amount of charge in integral form:

$$\oint_S \vec{D} \cdot d\vec{s} = \sum q \tag{1}$$

where $\vec{D}$ is the electric displacement vector; q is the amount of charge; s is the area of the closed surface.

In its differential form, the Gauss's theorem has the form

$$\nabla \cdot \vec{D} = \rho, \tag{2}$$

where ρ is the volume charge density.

For simplicity, we assume that the structure is homogeneous and has isotropic properties:

$$\varepsilon_x = \varepsilon_y = \varepsilon_z,$$

where ε is permittivity.

In this case, Equation (2) can be written as

$$\nabla \cdot \vec{E} = \frac{\rho}{\varepsilon}, \tag{3}$$

Taking into account the fact that the electric field strength can be represented as

$$\vec{E} = -\nabla\varphi, \tag{4}$$

Equation (3) takes the following form:

$$\nabla \cdot \nabla\varphi = -\frac{\rho}{\varepsilon}. \tag{5}$$

In the conventional form, Equation (5) can be represented as

$$\nabla^2 \varphi = -\frac{\rho}{\varepsilon}. \tag{6}$$

In the Cartesian coordinate system, Equation (6) is written as follows:

$$\frac{\partial}{\partial x}\left(\varepsilon\frac{\partial\varphi}{\partial x}\right) + \frac{\partial}{\partial y}\left(\varepsilon\frac{\partial\varphi}{\partial y}\right) + \frac{\partial}{\partial z}\left(\varepsilon\frac{\partial\varphi}{\partial z}\right) = -\rho. \tag{7}$$

Assuming that the VO_2 is surrounded by a layer of air, Equation (6) should be supplemented with the Laplace equation for the air gap:

$$\frac{\partial}{\partial x}\left(\varepsilon\frac{\partial\varphi}{\partial x}\right) + \frac{\partial}{\partial y}\left(\varepsilon\frac{\partial\varphi}{\partial y}\right) + \frac{\partial}{\partial z}\left(\varepsilon\frac{\partial\varphi}{\partial z}\right) = 0. \tag{8}$$

The solution of Equations (7) and (8) addresses a three-dimensional field distribution problem. In the general case, the coefficients ε and ρ exhibit nonlinear behavior, depending on both the magnitude and frequency of the current flowing through the VO_2 structure. Furthermore, the electrical conductivity and dielectric permittivity of VO_2 are strongly temperature-dependent, particularly near the well-known phase transition point of approximately 68 °C, during which these properties can change by several orders of

magnitude [28,29,40]. To incorporate these effects into the mathematical model, frequency- and temperature-dependent characteristics—specifically $\varepsilon(f)$, $R(f)$, $\varepsilon(T)$, and $R(T)$—were not measured directly but derived analytically by approximating reference data presented in previous studies [28–30,40]. These fitted analytical expressions were used as input parameters for the finite element simulation, ensuring consistency with experimentally observed material behavior without reproducing the original datasets in graphical form.

Equations (7) and (8) describe a stationary electric field that does not change over time. To analyze nonstationary electric fields caused by varying direct currents or alternating currents, we write down a system of Maxwell equations that determines the ratios for electric field strength $\vec{E}$, conduction current density $\vec{J}$ and electric displacement $\vec{D}$:

$$\nabla \times \vec{E} = 0; \tag{9}$$

$$\nabla \cdot \left(\vec{J} + \frac{\partial \vec{D}}{\partial t} \right) = 0; \tag{10}$$

$$\vec{J} = \sigma \vec{E}; \tag{11}$$

$$\vec{D} = \varepsilon \vec{E}. \tag{12}$$

where σ is the conductivity.

Substitute (11) and (12) into Equation (10). Taking into account (4) and (9), we obtain

$$-\nabla \cdot (\sigma \cdot \nabla \varphi) - \nabla \cdot \frac{\partial}{\partial t} (\varepsilon \cdot \nabla \varphi) = 0. \tag{13}$$

For a correct description of the problem under study, Equation (13) must be supplemented with Dirichlet boundary conditions

$$\varphi = \varphi_D \; on \; \Gamma_E \tag{14}$$

and Neumann boundary conditions

$$\left(\vec{J} + \frac{\partial \vec{D}}{\partial t} \right) \cdot \vec{n} = 0 \; on \; \Gamma_J.$$

where φ_D is the set value of the potential at the boundary Γ_E; $\vec{n}$ is the external unit vector of the normal to the boundary Γ_J.

Taking into account (4), the last condition takes the form

$$\left(\sigma \cdot \nabla \varphi + \frac{\partial}{\partial t} \varepsilon \cdot \nabla \varphi \right) \cdot \vec{n} = 0. \tag{15}$$

To solve the boundary value problem (13)–(15), we apply the Galerkin FEM [44], which assumes the approximation of the scalar potential by a linear combination of nodal basis functions of the form

$$\varphi \approx \varphi^{(n)} = \sum_{j=1}^{n} \varphi_j N_j + \sum_{j=n+1}^{n_{nd}} \varphi_j N_j, \tag{16}$$

where n_{nd} is the number of nodes in a finite element grid; n is the number of nodes that do not belong to Γ_E; φ_j—time potential functions in grid nodes; N_j—shape functions in grid nodes, $j = 1, 2, \ldots, n_{nd}$.

The second component of Equation (16) represents the known potentials at the boundary Γ_E:

$$\varphi_D = \sum_{j=n+1}^{n_{nd}} \varphi_j N_j.$$

Convert (16) to (13). To do this, multiply (16) by the functions of the form N_i, $i = 1, 2, \ldots, n$ and, integrating over the field of study Ω, we obtain a system of Galerkin equations:

$$\begin{array}{l} \sum\limits_{j=1}^{n} \varphi_j(t) \int\limits_{\Omega} \nabla N_i \cdot \sigma \cdot \nabla N_j \, d\Omega + \frac{d}{dt} \varphi_j(t) \int\limits_{\Omega} \nabla N_i \cdot \varepsilon \cdot \nabla N_j \, d\Omega = \\ = -\int\limits_{\Omega} \nabla N_i \cdot (\sigma \cdot \nabla \varphi_D + \frac{\partial}{\partial t} \varepsilon \cdot \nabla \varphi_D \Big) d\Omega, \;\; i = 1, 2, \ldots, n. \end{array} . \tag{17}$$

In matrix form, the system of Equation (17) has the form

$$[S_\sigma]\{\varphi(t)\} + \frac{d}{dt}([S_\varepsilon]\{\varphi(t)\}) = \{f(t)\}. \tag{18}$$

where $\{\varphi(t)\}$ is a vector consisting of unknown potential time functions; $\{f(t)\}$ is a vector consisting of elements of stiffness matrices; $[S_\sigma] = \sum\limits_{e=1}^{Ne} \left(\frac{\sigma}{4\Delta^e} [K]^e \right)$ is the matrix of the connection of the calculated area with σ; $[S_\varepsilon] = \sum\limits_{e=1}^{Ne} \frac{\varepsilon \, \Delta^e}{12} [Q]^e$ is the matrix of permeability accounting; e is the element of the studied area; N_e is the number of elements into which the calculated area is divided; Δ^e is the area of the element; i, j, k are the indices of the element.

The area of the element Δ^e is calculated as

$$\Delta^e = x_j y_k - y_j x_k + x_i y_j - x_i y_k + y_i x_k - y_i x_j.$$

The matrices $[K]^e$ and $[Q]^e$ are defined as follows:

$$[K]^e = \begin{bmatrix} (\beta_i^e)^2 + (\gamma_i^e)^2 & \beta_i^e \beta_j^e + \gamma_i^e \gamma_j^e & \beta_i^e \beta_k^e + \gamma_i^e \gamma_k^e \\ \beta_i^e \beta_j^e + \gamma_i^e \gamma_j^e & (\beta_j^e)^2 + (\gamma_j^e)^2 & \beta_j^e \beta_k^e + \gamma_j^e \gamma_k^e \\ \beta_i^e \beta_k^e + \gamma_i^e \gamma_k^e & \beta_j^e \beta_k^e + \gamma_j^e \gamma_k^e & (\beta_k^e)^2 + (\gamma_k^e)^2 \end{bmatrix}$$

$$[Q]^e = \begin{bmatrix} 2 & 1 & 1 \\ 1 & 2 & 1 \\ 1 & 1 & 2 \end{bmatrix}.$$

The coefficients of the matrix $[K]^e$ are determined by the formulas

$$\beta_i^e = y_j - y_k; \; \beta_j^e = y_k - y_i; \; \beta_k^e = y_i - y_j;$$

$$\gamma_i^e = x_k - x_j; \; \gamma_j^e = x_i - x_k; \; \gamma_k^e = x_j - x_i.$$

The solution of the system of Equation (18), as a rule, is performed in the form of a two-point approximation of the time derivative:

$$\frac{\partial \varphi}{\partial t} = \frac{\varphi_{t+\Delta t} - \varphi_t}{\Delta t},$$

and as a result, the Krank–Nicholson scheme can be applied [44].

To increase the calculation speed of the system of Equation (18), we represent the nonlinear dependences of conductivity and permeability in the form of analytical equations.

We implement the dependency $\varepsilon(f)$ in the form of a corresponding function using the Fortran language (Listing A1).

The coefficients a, b, c, and d were derived analytically.

A graphical interpretation of the characteristic $\varepsilon(f)$ constructed using the Listing A1 program is shown in Figure 1a, on a logarithmic scale—Figure 1b.

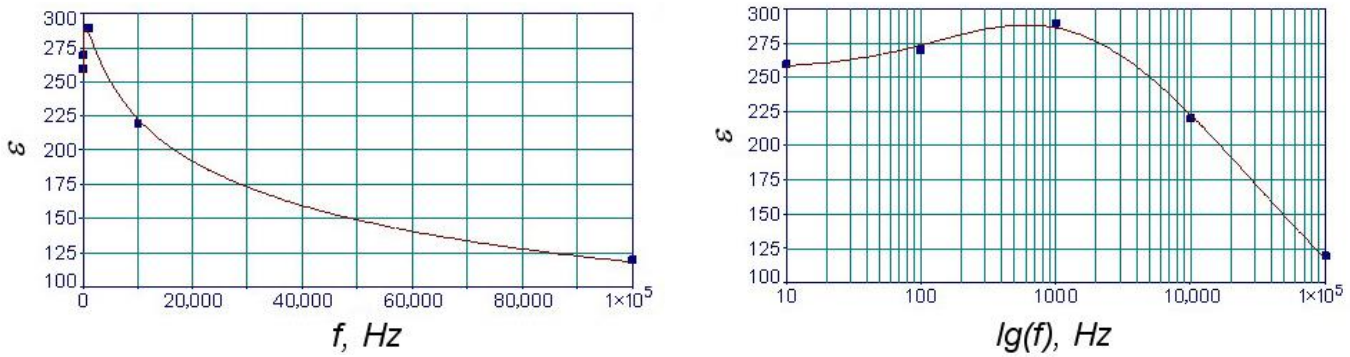

(**a**) (**b**)

Figure 1. The dependence of permeability on the frequency of the current on a linear scale (**a**) and on a logarithmic scale (**b**).

The coefficient of determination of the curve is $r^2 = 0.9976381811$.

Similarly, based on previously published experimental data [28,30], we formulated an analytical expression representing the dependence R (f) for the powder-based VO_2 structure:

$$R(f) = a + b \cdot f^{1.5} + c \cdot (\ln f)^2 + d \cdot f^{0.5}. \quad (19)$$

The coefficients of Equation (19) are $a = 1.551851749$, $b = -0.00096628$, $c = 0.001734340$, and $d = -0.03713498$, and the coefficient of determination $r^2 = 0.9999998864$.

Let us show (19) in the form of a graph (Figure 2).

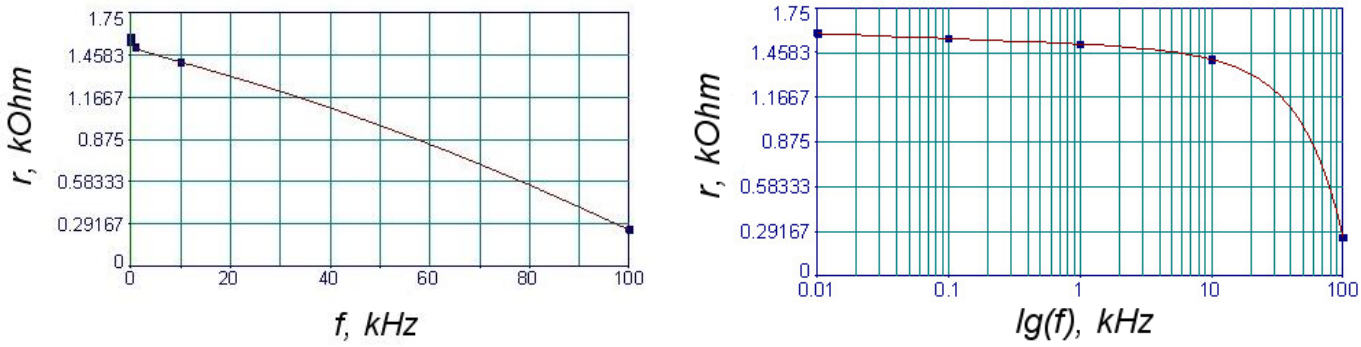

(**a**) (**b**)

Figure 2. Dependence of the resistance VO_2 structure on the frequency of the current: linear scale (**a**), logarithmic scale (**b**).

Since the formation of the metal–semiconductor phase transition in the VO_2 structure occurs at a certain temperature, let us describe the process of heat transfer by a parabolic-type heat conduction equation:

$$rC_p \frac{\partial T}{\partial t} - \nabla \cdot k \nabla T = Q, \quad (20)$$

where r is the density of the substance; C_p is the specific heat capacity; T is the temperature function; k is thermal conductivity of the substance; $Q = Q(x, y, z, t)$ is the power of the heat source.

Let us represent the temperature-dependent behavior of ε (T) using an analytical expression fitted to previously published experimental data [38]:

$$\varepsilon(T) = a + b \cdot T^{2.5} + c \cdot T^3, \quad (21)$$

where the coefficients of the polynomial are a = 20.31776117; $b = -2.8535^{-0.5}$; $c = 1.20045^{-0.5}$.

The coefficient of determination of Equation (21) is $r^2 = 0.9999978457$; the graph of the equation is shown in Figure 3.

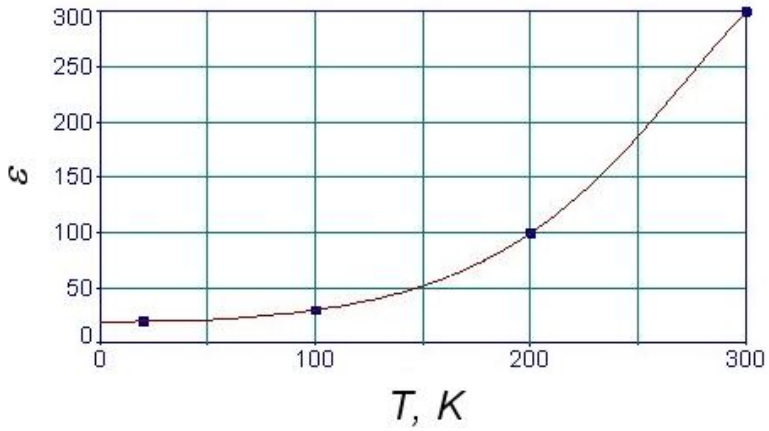

Figure 3. Dependence of permeability on temperature.

By analogy with (19), let us show the experimental dependence $R(T)$ in the form of a Fortran program implemented on the basis of two functions (Listing A2). The erf (x) function is called from the eqn (x) function during the calculation process. The input data for eqn (x) are the points of the graph $R(T)$.

In Figure 4, a graph $R(T)$ is shown using the functions erf (x) and eqn (x). The coefficient of determination of the model is $r^2 = 0.9650488282$, which allows us to conclude that the accuracy of the characteristic is acceptable.

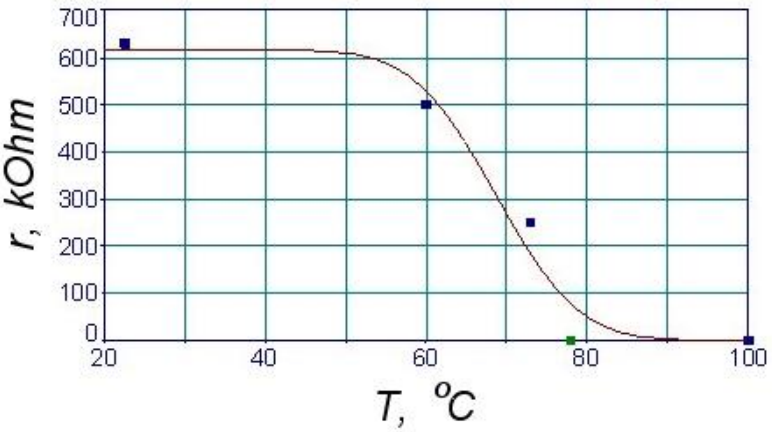

Figure 4. Dependence of the resistance of the structure VO_2 on temperature.

Elements based on VO_2 can be manufactured using ceramic technology from the material composition (weight %) [34]:

$$80\ \%\ VO_2 + 20\%\ P_2O_5.$$

where P_2O_5—diphosphorus pentoxide.

Experimental samples of thermistors, as a rule, have a cylindrical shape (Figure 5a) with a diameter of 10–12 mm and a height of 1–10 mm. Contacts are applied to the end surfaces by rubbing an indium–gallium eutectic. The appearance and dimensions of the investigated sample are presented in Figure 5b.

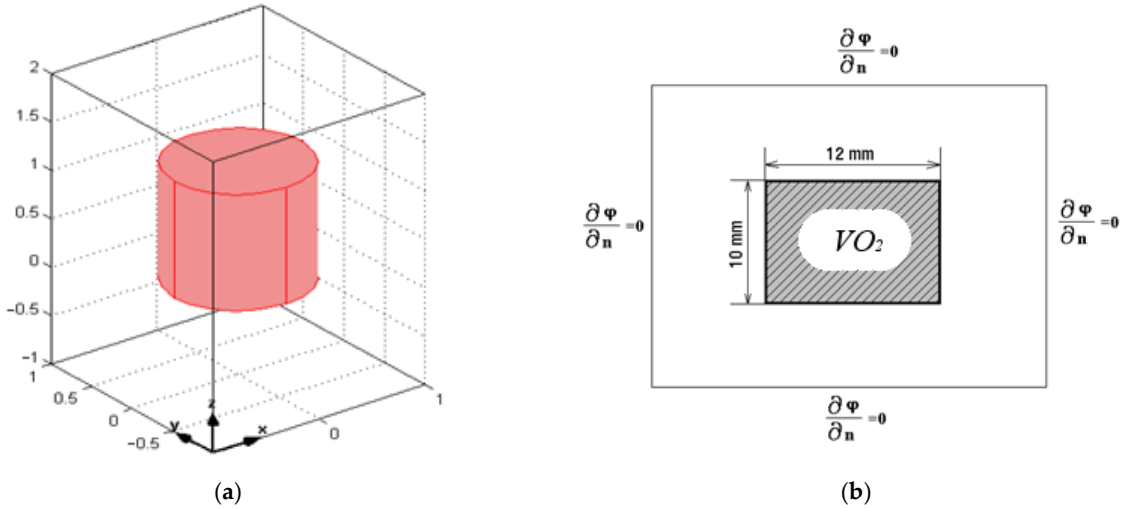

(**a**) (**b**)

Figure 5. Three-dimensional model (**a**) and boundary conditions of the VO_2 structure (**b**).

3. Results

Since only the conduction phase is considered at the initial stage of structural studies, we exclude thermal processes and nonlinear changes in permeability and conductivity from the study. Thus let us consider a complex solution of Equation (18), taking into account nonlinear dependencies of only electrical quantities in the three-dimensional VO_2 structure. To do this, we apply the finite element method [44].

The powder tablet is surrounded by an air gap of a cubic shape with dimensions 25 × 25 mm (Figure 5a). Figure 5b shows the boundary conditions of the model.

Applying the triangulation procedure of the computational domain, we obtain a discrete model. Triangulated parts of the air layer and the powder tablet are shown in Figure 6.

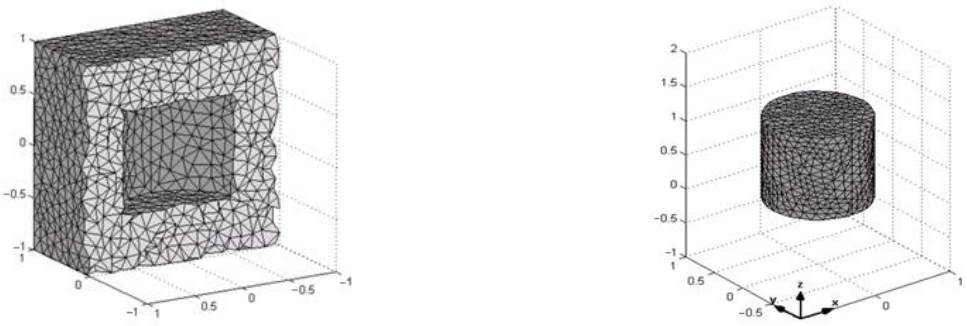

(**a**) (**b**)

Figure 6. Triangulated models of the air gap around the powder tablet (**a**) and vanadium dioxide structure (**b**).

The calculation was performed for the conductive phase of the VO_2 tablet with RMS voltage 220 V, 50 Hz. The voltage is applied to the upper and lower planes of the tablet.

The VO_2 structure is connected in series with the primary winding of the transformer with a transformation ratio $k_u = \frac{U_1}{U_2} = 14$ (Figure 7).

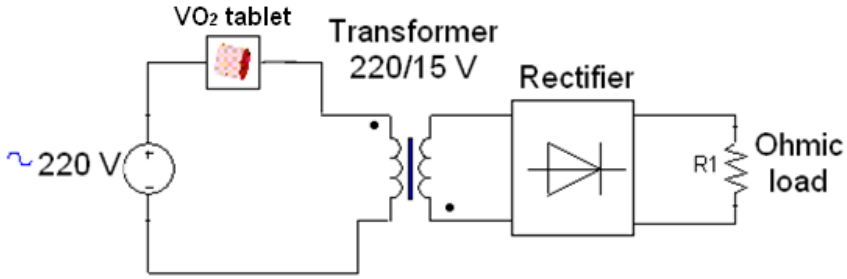

Figure 7. A circuit-field model for VO_2 structure research.

The transformer feeds a simple electrical circuit with a rectifier and an ohmic load $R_1 = 15$ Ohms.

Thus, the considered model includes both a circuit model and the finite element model of a VO_2 structure.

The considered model is calculated as a time-dependent problem in the time interval $t_{calc} = 160$ ms. The calculation time was chosen because of the need to consider the entire transition process, which includes several full periods.

As a result, the distribution of the electric field strength in the VO_2 structure at each point of the time interval is obtained. As an example, Figure 8 shows the distribution of the electric field strength at a time point of 25 ms.

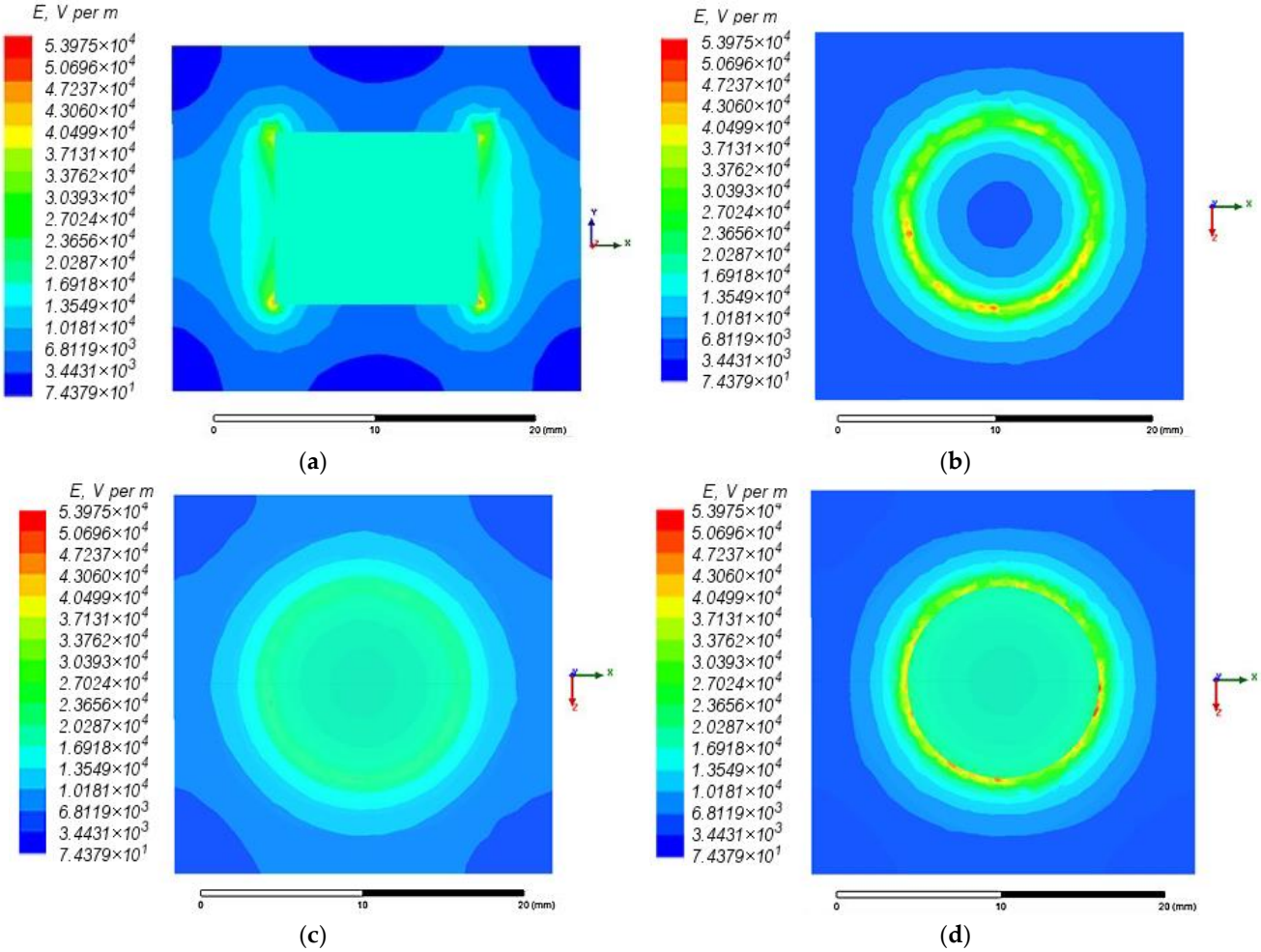

Figure 8. Distribution of the electric field strength (RMS voltage 220 V): (**a**) cross-section of the tablet; (**b**) the lower surface; (**c**) section by height h = 5 mm; (**d**) the upper surface.

The results of simulation the electric field strength distribution show that at a frequency of 50 Hz, the field concentration occurs mainly on the surface of the structure, reaching a value of $5 \cdot 10^4$ V/m. This effect is pronounced on the surface at the place where the positive potential is applied. In the internal structure, the distribution of electric field is uniform and reaches values of 2×10^4 V/m. Increasing the frequency of the current flowing through the structure enhances this effect.

For a detailed analysis of the processes occurring in the conduction mode of the VO_2 structure, a series of experimental studies aimed at studying the shape of the current flowing through the powder tablet and the primary winding of the transformer has been carried out (Figure 9).

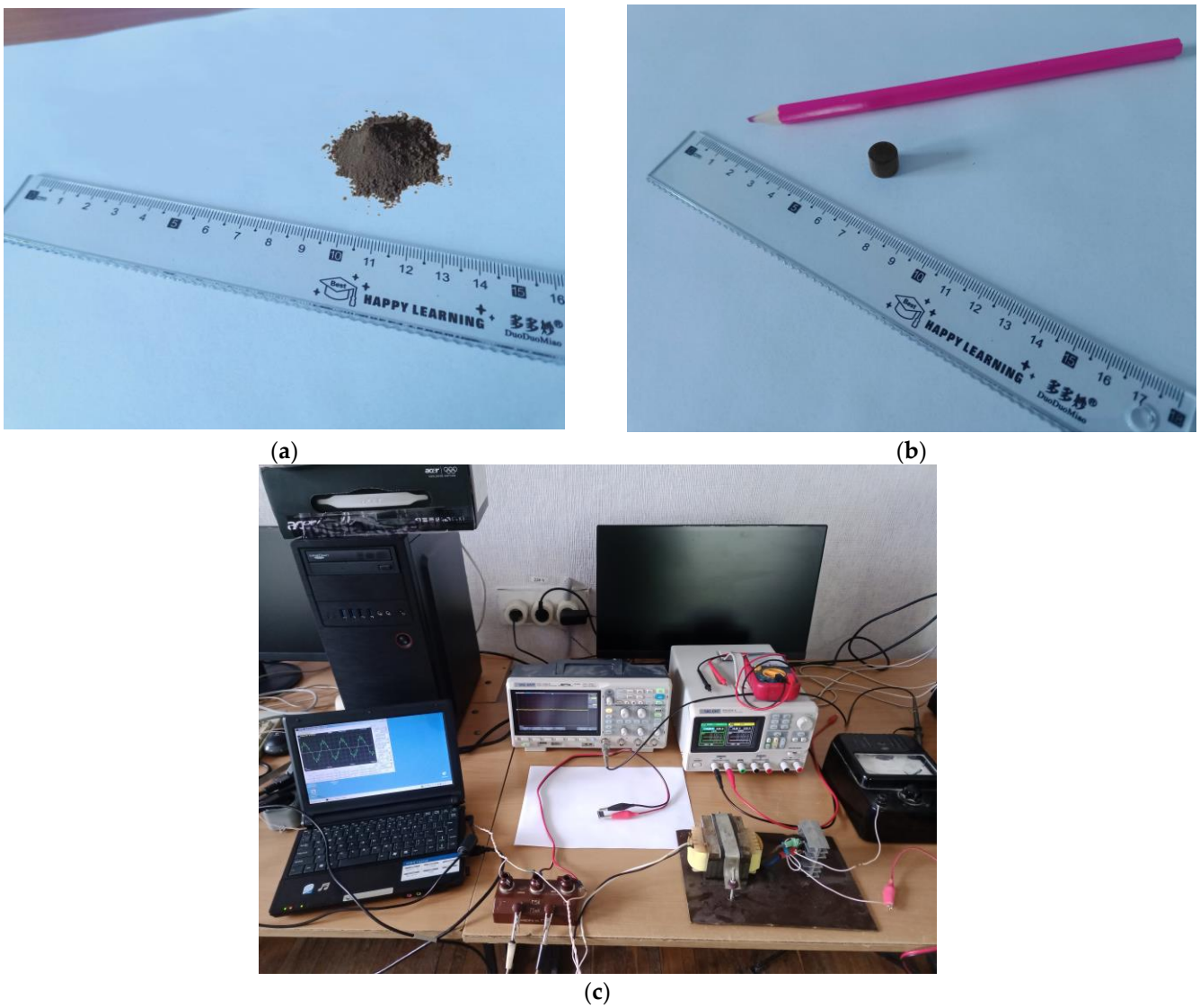

(**a**) (**b**)

(**c**)

Figure 9. Laboratory studies of the conductive properties of vanadium dioxide: (**a**) initial VO_2 powder before pressing; (**b**) resulting VO_2 tablet after pressing and thermal treatment; (**c**) experimental setup for measuring the electrical characteristics of the VO_2 structure using an oscilloscope, signal generator, and power supply.

As a result of the experiment, an oscillogram of the current flowing through the VO_2 structure was obtained (Figure 10a). As can be seen, the current reaches a value of about 0.3 A. At the same time, the current shape has slight distortions in the peak range, which can be explained by the saturation processes of steel in the transformer.

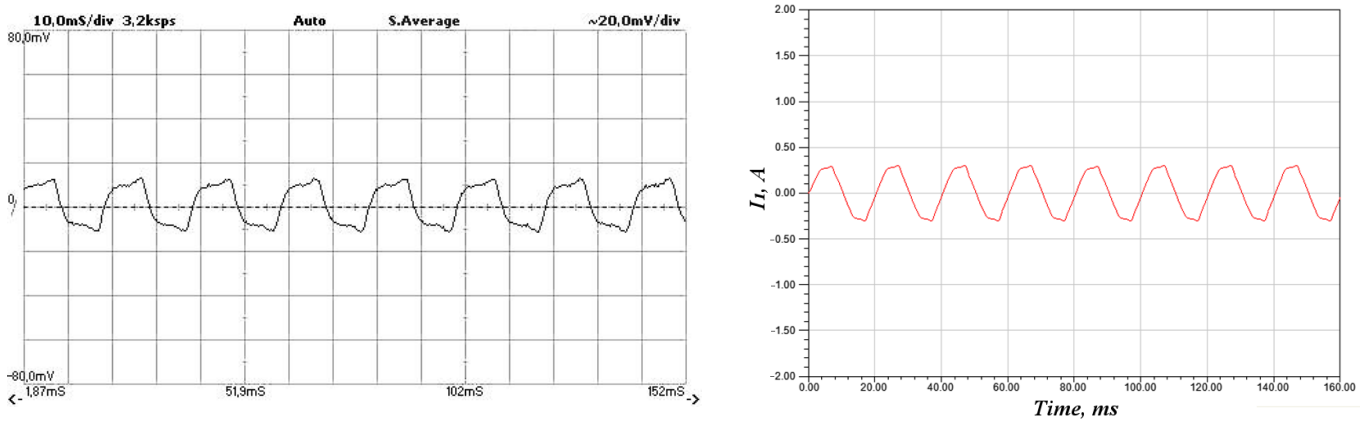

(**a**) (**b**)

Figure 10. The experimental oscillogram of the VO_2 structure current (**a**) (vertical axis division value 20 mV/div, horizontal axis division value 10 mS/div, limit parameters of the measuring shunt 1.5 A at 75 mV, maximum signal swing 14 mV, calculated current value 0.28 A) and calculated current of the thermistor obtained with the FEM model (**b**).

For comparison, Figure 10b shows a graph of the VO_2 structure current, obtained by calculation. It follows from the graph that the current is sinusoidal, and in the peak range, there is a slight distortion of the current shape. The difference in the signal distortion of the calculated and experimental data is explained by the complex nature of the inductance change in the primary winding of the transformer. At the same time, the peak current values reach a value of about 0.3 A, which is in good agreement with the experimental data.

A comparison of calculated and experimental data allows us to conclude that the developed model is adequate and allows us to study transients in semiconductor powdery structures.

4. Discussion

The presented mathematical model describes a semiconductor structure based on vanadium dioxide in the conduction phase. A special feature of the model is the combination of circuit and field equations. This model is simplified because it has a number of assumptions. In particular, only the conduction phase is considered without switching to the dielectric mode. In addition, thermal processes in the VO_2 structure are not taken into account.

In addition, the model takes into account the nonlinear changes of the permeability and conductivity of the vanadium dioxide structure depending on the frequency of the current. In particular, equations describing the dependences $\varepsilon(f)$ and $R(f)$ with high accuracy are obtained.

The results allow us to conclude that in the conduction mode, a semiconductor structure based on vanadium dioxide has conductive properties similar to conventional conductive materials, such as copper or aluminum, as evidenced by the obtained graph of transient current in the electrical circuit. The simulation showed that at a frequency of 50 Hz, the concentration of charges on the surface of the VO_2 structure already significantly exceeds the number of charges inside the structure (Figure 10). Increasing the frequency of the current flowing through the powder tablet enhances this effect.

In addition, laboratory studies have shown that the inclusion of a semiconductor structure of vanadium dioxide at temperatures below 68 °C in an electric circuit of a sinusoidal current does not significantly affect the current flow.

This conclusion is confirmed by an experiment oscillogram (Figure 10a). The study showed that the sinusoidal current flowing in an electric circuit reaches a value of 0.3 A,

and the current shape is distorted when peak values are reached. Almost identical results were obtained when simulating a similar electrical circuit (Figure 10b). The deviation of the calculated current values is minimal and does not exceed 5–8%.

Based on the results obtained, it can be concluded that the created mathematical model of a VO_2 structure in the conduction mode is correct and can be used in further studies.

To position the present findings in the context of existing research, a comparative analysis with related works is warranted. Compared to previous studies on VO_2-based switching and protection elements, the presented results offer both complementary insights and distinct modeling advantages. In [13], the authors provided a comprehensive review of VO_2 switching devices, highlighting their fast response (~ns), endurance over 260 million cycles, and potential in printed electronics. However, no modeling or simulation results are included in that work. By contrast, our study introduces a fully validated FEM-based 3D model with experimental agreement (error below 8%) and precise parameter fits (R^2 = 0.998–0.999), delivering a quantitative framework missing from [13].

The authors of [14] experimentally demonstrated VO_2-based multibridge current limiters exhibiting abrupt phase transitions induced by Joule heating. Their devices function as resettable protectors, where switching arises from local thermal effects. While [14] provides valuable empirical results, it does not include field-based numerical simulations. Our model, though currently limited to the conductive phase and excluding thermal feedback, complements [14] by offering a spatially resolved, parameter-fitted simulation framework that can serve as a foundation for future thermo-electrical coupling models.

The authors of [15] reported nanosecond-scale threshold switching and self-oscillating behavior in VO_2, supported by phenomenological modeling of negative differential resistance. Their work focuses on describing dynamic transition phenomena, including S-type I–V characteristics and high-frequency generation up to 300 MHz. Our study does not currently reproduce such behaviors due to its restriction to a single (conductive) phase, but it introduces a physically consistent model based on material properties and electric field distribution—something not addressed in [15].

In [16], the authors investigated strain-induced tuning of the VO_2 transition temperature, showing the ability to shift T_t by modifying the crystal structure. While their work is essential in material-level design, it does not address electrical modeling or protective device behavior. Our model assumes constant material parameters and does not yet incorporate structural tunability, though such extensions are feasible within the same framework.

In [17], the authors focused on the optical and mechanical characteristics of VO_2 and their dependence on phase state. Their study provides theoretical and experimental support for multifunctional VO_2 applications but lacks an electrical or circuit-level model. Our model focuses specifically on the electrical behavior under AC excitation and nonlinear conduction, filling a different niche complementary to [17].

The authors of [18] reported ultrafast electrical switching in VO_2-based devices under sub-nanosecond pulses. Their results confirm the possibility of dynamic switching in highly confined geometries. However, no numerical simulations are provided, and the switching behavior remains experimentally observed rather than computationally analyzed. In contrast, our model—although limited to steady-state AC excitation—lays the groundwork for future transient modeling by introducing a spatial FEM framework capable of integration with time-domain solvers.

Additionally, the authors of [19] demonstrated fast and reversible resonant switching behavior in VO_2 thin films under high-frequency excitation (~13.56 MHz), driven by a combination of the metal–insulator transition and circuit resonance. While their work illustrates advanced functional behavior in VO_2 structures, it is primarily experimental and lacks

quantitative modeling of electric field distributions or device-scale simulations. Our model, although not addressing high-frequency resonance or dynamic bistability, introduces a spatially resolved field-based approach that could be extended to such applications.

The authors of [22] proposed a simplified thermal switching model for VO_2, describing transition thresholds and state-dependent resistance behavior under varying temperature and voltage conditions. However, their model does not resolve the spatial structure or field distribution within the VO_2 device, nor does it employ a FEM framework. In contrast, our work incorporates 3D field distributions, boundary conditions, and device geometry, enabling detailed visualization of the current paths and field enhancement—features not accessible in the lumped-element models used in [22].

These comparisons reinforce that while prior studies [13–19,22] have provided valuable insights into experimental switching phenomena, device fabrication, material tuning, and approximate behavioral modeling of VO_2 structures, the present work uniquely contributes a numerically verified, physically consistent FEM-based simulation of the conductive phase, with strong correlation to experimental data. Future developments will aim to extend this model to incorporate phase transitions and thermal dynamics to align more closely with the full range of phenomena observed in the literature.

5. Conclusions

In this study, a mathematical model of a vanadium dioxide (VO_2) semiconductor structure operating in its conductive phase was presented. Developed with the finite element method (FEM), the model enables calculation of the electric field distribution inside the structure under a low-frequency (50 Hz) AC voltage. Numerical simulations showed that the maximum electric field strength at the surface reaches about 5×10^4 V m^{-1}, whereas inside the structure, the field remains more uniform at roughly 2×10^4 V m^{-1}.

Experimental tests confirmed the model's adequacy. The peak current obtained both experimentally and numerically was approximately 0.3 A. Minor waveform distortions at the current peaks—no greater than 5–8—were attributed to complex electromagnetic effects in the transformer core (specifically, magnetic saturation) that were not fully captured in the model.

A key feature of the model is its treatment of the nonlinear dependence of VO_2's electrical properties on frequency and temperature. Analytical expressions for magnetic permeability and resistance were derived with high accuracy: the coefficients of determination (R^2) for permeability-versus-frequency and resistance-versus-frequency are 0.9976 and 0.9999, respectively.

The authors note several limitations: only the conductive phase was modeled (no transition to the insulating phase is considered), and thermal effects—which can strongly influence device behavior in practice—were omitted.

Overall, the proposed model is effective and reliable within the conductive phase, yet more comprehensive descriptions of phase transitions and thermal phenomena are needed for full realism, which is the subject of further research. The results underscore the promise of VO_2-based structures for protecting electronic equipment against current surges, providing fast response and operational stability.

Author Contributions: Methodology, V.K. (Vitalii Kuznetsov); Software, O.K.; Formal analysis, V.K. (Valeriy Kuznetsov); Investigation, M.T.; Writing—original draft, S.K.; Writing—review & editing, P.H.; Visualization, A.R. All authors have read and agreed to the published version of the manuscript.

Funding: This research received no external funding.

Data Availability Statement: Data are contained within the article.

Conflicts of Interest: The authors declare no conflict of interest.

Appendix A

Listing A1. Fortran function for graphical interpretation of the characteristic $\varepsilon(f)$.

```
real function eqn (x)
!--------------------------------------
real :: a = 288.233, b = 604.124
real :: c = 55928.927, d = 77.398
!--------------------------------------
real x,y
real n
real m
n = log(1.0 + (x − b) * (d * d − 1.0)/(c * d))
m = log(d)
y = a * exp (−0.693 * n * n/(m * m))
eqn = y
return.
```

Listing A2. Two functions of a Fortran program for experimental dependence $R(T)$.

```
real function erf (x)
!---------------------
real x
real t,ax,y
ax = abs (x)
if (ax.gt.5.94) then
if (x.lt.0.0) then
erf = −1.0
else
erf = 1.0
end if
return
end if
t = 1/(1 + 0.5 * ax)
y = (−1.265 + t * (2.413 + t * (−9.923 + t * (13.302 + t * (−24.319 + t * (23.692 + t * (−22.19 + &
&t * (17.33 + t * (−6.393 + t * (6.048 + t * (0.281 + t * (0.938 + t*0.082))))))))))/(1 + t *
(−1.11 + &
&t * (7.25 + t * (−5.043 + t * (17.240 + t * (−6.152 + t * (17.016 + t * (−1.320 + t * (7.6 + t *
(0.929 + t * (1.484 + &
&t * (0.245 + t * 0.069)))))))))))
If (x.ge.0) then
erf = 1 − t * exp (−x * x + y)
else
erf = −1 + t * exp(−x * x + y)
end if
return
end
!-----------------------------
real function eqn (x)
!-----------------------------
real :: a = 616.195, b = 68.766
```

```
real :: c = −8.132
!-----------------------------
real x,y
real n
real erf
n = (x − b)/(1.414 * c)
y = a * 0.5 * (1.0 + erf (n))
eqn = y
return.
```

References

1. Okilly, A.H.; Kim, N.; Baek, J. Inrush Current Control of High Power Density DC–DC Converter. *Energies* **2020**, *13*, 4301. [CrossRef]
2. Smugala, D.; Bonk, M. Modeling of Inrush Current Surges-LED Strip Drivers Case Study. *Energies* **2023**, *16*, 1473. [CrossRef]
3. Łukaniszyn, M.; Baron, B.; Kolańska-Płuska, J.; Majka, Ł. Inrush Current Reduction Strategy for a Three-Phase Dy Transformer Based on Pre-Magnetization of the Columns and Controlled Switching. *Energies* **2023**, *16*, 5238. [CrossRef]
4. Li, C.; Yang, Y.; Li, W.; Li, H. A Soft-Start-Based Method for Active Suppression of Magnetizing Inrush Current in Transformers. *Electronics* **2023**, *12*, 3114. [CrossRef]
5. Gao, T.; Wang, Y.; Gao, Y.; Sun, G.; Wang, H.; Hou, J. Hybrid Control-Based Closed-Loop Soft Start-Up Method for LLC Resonant Converters. *Electronics* **2023**, *12*, 4563. [CrossRef]
6. Rini, M.; Hao, Z.; Schoenlein, R.W. Optical switching in VO_2 films by below-gap excitation. *Appl. Phys. Lett.* **2008**, *92*, 181904. [CrossRef]
7. Subrahmanyam, A.; Reddy, Y.B.K.; Nagendra, C.L. Nano-vanadium oxide thin films in mixed phase for microbolometer applications. *J. Phys. D Appl. Phys.* **2008**, *41*, 195108. [CrossRef]
8. Huffman, T.J.; Hendriks, C.; Walter, E.J.; Yoon, J.; Ju, H.; Smith, R.; Carr, G.L.; Krakauer, H.; Qazilbash, M.M. Insulating phases of vanadium dioxide are Mott-Hubbard insulators. *Phys. Rev. B* **2017**, *95*, 075125. [CrossRef]
9. Lin, J.; Ji, H.; Swift, M.W.; Hardy, W.J.; Peng, Z.; Fan, X.; Nevidomskyy, A.H.; Tour, J.M.; Natelson, D. Hydrogen diffusion and stabilization in single-crystal VO_2 micro/nanobeams by direct atomic hydrogenation. *Nano Lett.* **2014**, *14*, 5445–5451. [CrossRef]
10. Yoon, H.; Choi, M.; Lim, T.W.; Kwon, H.; Ihm, K.; Kim, J.K.; Choi, S.Y.; Son, J. Reversible phase modulation and hydrogen storage in multivalent VO_2 epitaxial thin films. *Nat. Mater.* **2016**, *15*, 1113–1119. [CrossRef]
11. Fisher, B.; Genossar, J.; Reisner, G.M. Systematics in the metal-insulator transition temperatures in vanadium oxides. *Solid State Commun.* **2016**, *226*, 29–32. [CrossRef]
12. Hansmann, P.; Toschi, A.; Sangiovanni, G.; Saha-Dasgupta, T.; Lupi, S.; Marsi, M.; Held, K. Mott–Hubbard transition in V_2O_3 revisited. *Phys. Status Solidi B* **2013**, *250*, 1251–1264. [CrossRef]
13. Darwish, M.; Zhabura, Y.; Pohl, L. Recent Advances of VO_2 in Sensors and Actuators. *Nanomaterials* **2024**, *14*, 582. [CrossRef] [PubMed]
14. Gao, X.; Roskamp, T.J.; Swoboda, T.; Rosário, C.M.; Smink, S.; Muñoz Rojo, M.; Hilgenkamp, H. Multibridge VO_2-Based Resistive Switching Devices in a Two-Terminal Configuration. *Adv. Electron. Mater.* **2023**, *9*, 2300304. [CrossRef]
15. Pergament, A.; Velichko, A.; Belyaev, M.; Putrolaynen, V. Electrical switching and oscillations in vanadium dioxide. *Phys. B Condens. Matter* **2018**, *536*, 239–248. [CrossRef]
16. Nag, J.; Haglund, R.F., Jr. Synthesis of vanadium dioxide thin films and nanoparticles. *J. Phys. Condens. Mater.* **2008**, *20*, 264016. [CrossRef]
17. Schoiswohl, J.; Surnev, S.; Netzer, F.P.; Kresse, G. Vanadium Oxide Nanostructures: From Zero- to Three-Dimensional. *J. Phys. Condens. Matter* **2006**, *18*, R1. [CrossRef]
18. Basyooni, M.A.; Al-Dossari, M.; Zaki, S.E.; Eker, Y.R.; Yilmaz, M.; Shaban, M. Tuning the Metal–Insulator Transition Properties of VO_2 Thin Films with the Synergetic Combination of Oxygen Vacancies, Strain Engineering, and Tungsten Doping. *Nanomaterials* **2022**, *12*, 1470. [CrossRef]
19. Yoon, J.; Hong, W.-K.; Kim, Y.; Park, S.-Y. Nanostructured Vanadium Dioxide Materials for Optical Sensing Applications. *Sensors* **2023**, *23*, 6715. [CrossRef]
20. Berezina, O.Y.; Artyukhin, D.V.; Velichko, A.A.; Pergament, A.L.; Kuldin, N.A.; Khomlyuk, N.P.; Sergeyeva, O.V. Metal–Semiconductor Phase Transition in Undoped and Doped Vanadium Dioxide Films. *Condens. Matter Interphases* **2009**, *11*, 194–201.
21. Shadrin, E.B.; Ilyinskiy, A.V. The nature of the metal–semiconductor phase transition in vanadium dioxide. *Phys. Solid State* **2000**, *42*, 1092–1099. [CrossRef]

22. Schneider, K.; Lubecka, M.; Czapla, A. V_2O_5 thin films for gas sensor applications. *Sens. Actuators B Chem.* **2016**, *236*, 970–977. [CrossRef]
23. Ilyinskiy, A.V.; Kvashenkina, O.E.; Shadrin, E.B. Phase Transition and Correlation Effects in Vanadium Dioxide. *Semiconductors* **2012**, *46*, 439–446. [CrossRef]
24. Joushaghani, A.; Jeong, J.; Paradis, S.; Alain, D.; Aitchison, J.S.; Poon, J.K.S. Characteristics of the Current-Controlled Phase Transition of VO_2 Microwires for Hybrid Optoelectronic Devices. *Photonics* **2015**, *2*, 916–932. [CrossRef]
25. Bleu, Y.; Bourquard, F.; Barnier, V.; Loir, A.-S.; Garrelie, F.; Donnet, C. Towards Room Temperature Phase Transition of W-Doped VO_2 Thin Films Deposited by Pulsed Laser Deposition: Thermochromic, Surface, and Structural Analysis. *Materials* **2023**, *16*, 461. [CrossRef]
26. Song, X.; Xu, Z.; Wei, D.; Yue, X.; Zhang, T.; Zhang, H.; Zhang, J.; Dai, Z.; Yao, J. Application of W-Doped VO_2 Phase Transition Mechanism and Improvement of Hydrophobic Self-Cleaning Properties to Smart Windows. *Photonics* **2023**, *10*, 1198. [CrossRef]
27. Semenov, A.L. Photoinduced Semiconductor–Metal Phase Transition and Switching Wave in a Vanadium Dioxide Thin Film. *Phys. Solid State* **2011**, *53*, 361–363. [CrossRef]
28. Tutov, E.A.; Kryukov, P.I.; Zlomanov, V.P. AC Conductivity Features of Polycrystalline Vanadium Dioxide. *Condens. Matter Interphases* **2002**, *16*, 220–224.
29. Mansingh, A.; Singh, R.; Sayer, M. Low frequency dielectric relaxation in lightly doped VO_2 single crystals. *Phys. Status Solidi A* **1978**, *49*, 773–779. [CrossRef]
30. Pergament, A.L.; Kuldin, N.A.; Stefanovich, G.B.; Velichko, A.A. Dielectric Properties of Vanadium Dioxide and Prospects for Using VO_2-Based Sandwich Structures in Sensor Technology. Modern problems of science and education. *Mod. Probl. Sci. Educ.* **2014**, *5*, 790.
31. Jaramillo, R.; Ha, S.D.; Silevitch, D.M.; Ramanathan, S. Origins of bad-metal conductivity and the insulator–metal transition in the rare-earth nickelates. *Nat. Phys.* **2014**, *10*, 304–307. [CrossRef]
32. Pergament, A.L.; Boriskov, P.P.; Kuldin, N.A.; Velichko, A.A. Electrical conductivity of vanadium dioxide switching channel. *Phys. Status Solidi B Basic Res.* **2010**, *247*, 2213–2217. [CrossRef]
33. Sher, E.M. Thermoelectric Converters of Electrical and Optical Signals—A New Class of Thermoelectric Devices. *Thermoelectricity* **2007**, *6*, 3–10.
34. Chernenko, I.M.; Tristan, O.N.; Ivon, A.I. Device for Protecting Incandescent Lamps from Inrush Current. Patent No. 49195, 16 September 2002. Available online: https://sis.nipo.gov.ua/uk/search/detail/358916/ (accessed on 13 June 2025).
35. Ivon, A.I.; Tristan, O.N.; Chernenko, I.M. Pulse Signal Delay Device. Patent No. 48396, 15 August 2002. Available online: https://sis.nipo.gov.ua/uk/search/detail/358247/ (accessed on 14 June 2025).
36. Bank, R.E.; Bürgler, J.F.; Fichtner, W.; Smith, R.K. Some upwinding techniques for finite element approximations of convection-diffusion equations. *Numer. Math.* **1990**, *58*, 185–202. [CrossRef]
37. Bank, R.E.; Rose, D.; Fichtner, W. Numerical methods for semiconductor device simulation. *SIAM J. Sci. Stat. Comput.* **1983**, *4*, 416–435. [CrossRef]
38. Brezzi, F.; Marini, L.D.; Pietra, P. Numerical simulation of semiconductor devices. *Comput. Methods Appl. Mech. Eng.* **1989**, *75*, 493–514. [CrossRef]
39. Mauri, A.; Bortolossi, A.; Novielli, G.; Sacco, R. 3D Finite Element Modeling of Current Densities in Semiconductor Transport with Impact Ionization. *J. Math. Ind.* **2015**, *5*. [CrossRef]
40. Tutov, E.A.E.; Manannikov, A.V.; Al-Khafaji, H.I.; Zlomanov, V.P. Surface and bulk conductivity of vanadium dioxide. *J. Tech. Phys.* **2017**, *87*, 367–371. [CrossRef]
41. Wang, Y.; Wang, L.; Gu, J.; Yan, X.; Lu, J.; Dou, S.; Li, Y.; Wang, L. Analysis of Thermal Stress in Vanadium Dioxide Thin Films by Finite Element Method. *Nanomaterials* **2022**, *12*, 4262. [CrossRef]
42. Oguntoye, I.O.; Padmanabha, S.; Hinkle, M.; Koutsougeras, T.; Ollanik, A.J.; Escarra, M.D. Continuously Tunable Optical Modulation Using Vanadium Dioxide Huygens Metasurfaces. *ACS Appl. Mater. Interfaces* **2023**, *15*, 41141–41150. [CrossRef] [PubMed] [PubMed Central]
43. Wang, Y.; Chen, Y.; Liu, F.; Chen, L.; Ji, K.; Wang, X.; Ji, X. Vanadium dioxide enabled polarization insensitive tunable broadband terahertz metamaterial absorber. *Sci. Rep.* **2025**, *15*, 10140. [CrossRef]
44. Segerlind, L.J. *Applied Finite Element Analysis*, 2nd ed.; Wiley: Hoboken, NJ, USA, 1976.